

Taming the expressiveness of neural-network wave functions for robust convergence to quantum many-body states

Dezhe Z. Jin*

Department of Physics and the Center for Theory of Emergent Quantum Matter,
Pennsylvania State University
University Park, PA 16802, USA †

(Dated: March 18, 2026)

Neural networks are emerging as a powerful tool for determining the quantum states of interacting many-body fermionic systems. The standard approach trains a neural-network ansatz by minimizing the mean local energy estimated from Monte Carlo samples. However, this typically results in large sample-to-sample fluctuations in the estimated mean energy and thus slow convergence of the energy minimization. We propose that minimizing a logarithmically compressed variance of the local energies can dramatically improve convergence. Moreover, this loss function can be adapted to systematically obtain the energy spectrum across multiple runs. We demonstrate these ideas for spin-1/2 particles in a 2D harmonic trap with attractive Pöschl–Teller interactions between opposite spins.

Introduction.—Variational quantum Monte Carlo (VMC) is a widely used technique for solving many-body wave functions of interacting quantum particles, including electrons in single atoms and molecules [1], electrons in condensed matter systems [2, 3], and ultra-cold atomic gases in optical traps [4]. The method seeks to optimize a trial wave function $\Psi_\theta(\mathbf{r})$ in the parameter space θ . Using Monte Carlo algorithms [5], particle configurations are sampled from the probability distribution defined by the trial wave function, and the local energy E_L is evaluated for each configuration. The local energy is defined as $E_L(\mathbf{r}; \theta) = \Psi_\theta^{-1} H \Psi_\theta$, where H is the Hamiltonian. The mean \bar{E}_L of the local energy serves as an estimator of the variational energy associated with the trial wave function. Minimizing \bar{E}_L can therefore be viewed as optimizing the trial wave function according to the variational principle [2].

For an eigenstate, E_L is constant across all samples. Therefore, the trial wave function can also be optimized by minimizing the variance σ_L^2 of the local energy [6, 7]. This is known as the zero-variance principle [6]. In the early days of VMC, direct minimization of \bar{E}_L was considered unstable; consequently, minimization of σ_L^2 was favored [7, 8]. However, it was later shown that the derivative of \bar{E}_L with respect to the parameters θ can be written in a form that reduces fluctuations arising from finite sampling, thereby making energy minimization more stable [9]. This shifted the field away from variance minimization toward energy minimization, which is now the default approach in VMC.

With the rapid advancement of artificial intelligence (AI), neural networks (NNs) have emerged as powerful ansätze for constructing trial wave functions [10–15]. Their high expressiveness helps overcome the limitations of the hand-crafted trial wave functions traditionally used

in VMC. Furthermore, these approaches are naturally well-suited to GPU architectures, enabling efficient and scalable simulations.

In this paper, we show that the expressiveness of NN wave functions can pose a significant challenge for energy-minimization approaches. Specifically, NN wave functions may exhibit a *plateau-edge (PE) property* in configuration space, characterized by relatively flat regions connected by sharp edges. In the flat regions, the potential energy can dominate over the kinetic energy, whereas the sharp edges contribute disproportionately to the kinetic energy. With a finite number of samples, the sharp-edge regions may be missed entirely, yielding an estimate of \bar{E}_L that is artificially small and can even fall below the true ground-state energy. Conversely, when the edges are sampled, \bar{E}_L can become large. This leads to large sample-to-sample fluctuations in \bar{E}_L , making energy minimization difficult and highly sensitive to the initialization of the NN parameters.

We propose minimizing the logarithmically compressed variance as an alternative objective. We show that this loss function enables robust convergence from a wide range of NN initializations, despite the PE property. The energy spectrum can be obtained through multiple runs, with the loss function modified to exclude energies found in previous runs.

Methods.— We study a system of spin- $\frac{1}{2}$ fermions confined in a two-dimensional harmonic trap. Attractive Pöschl–Teller interactions [16] are present between particles of opposite spin, while particles with the same spin do not interact. Such systems can be realized in cold atom experiments [17]. The Hamiltonian is given by

$$H = \sum_{i=1}^N \frac{1}{2} (-\nabla_i^2 + r_i^2) - \sum_{i=1}^{N_\uparrow} \sum_{j=1}^{N_\downarrow} \frac{\gamma}{\cosh^2(\mu|\mathbf{r}_i - \mathbf{r}_j|)}.$$

Here, N_\uparrow and N_\downarrow denote the numbers of spin-up and spin-down particles, respectively, with $N = N_\uparrow + N_\downarrow$. The parameters $\gamma > 0$ and $\mu > 0$ characterize the strength and

* dzj2@psu.edu

† <http://www.dezhejinlab.org/>

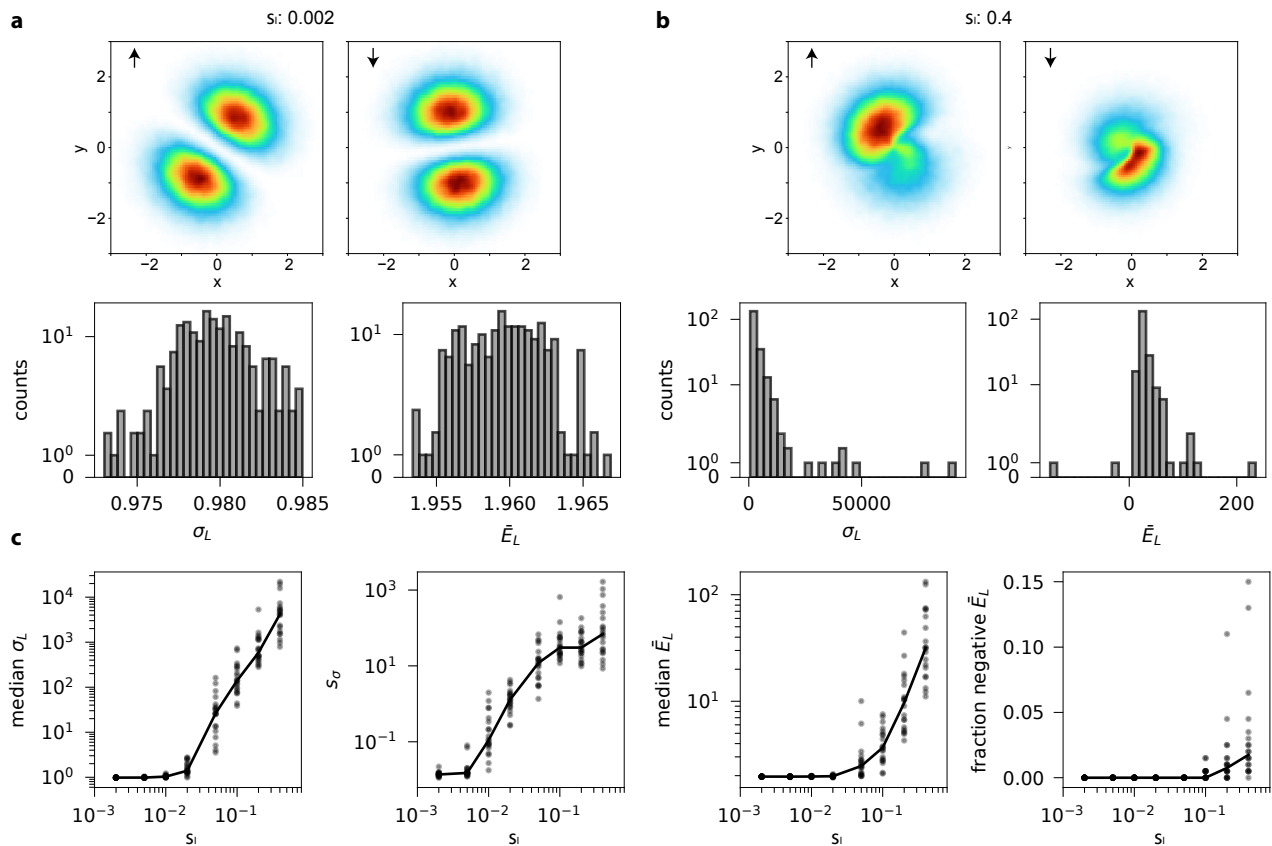


FIG. 1. **PE and PBE properties of NN wave functions.** **a.** Spatial distributions of up- and down-spin particles and the distributions of σ_L and \bar{E}_L for $s_I=0.002$. The distributions are obtained from 200 sets of 200,000 Monte Carlo samples. The spatial distributions are taken from one representative set. **b.** Same as **a** but for $s_I=0.4$. **c.** Median σ_L , spread s_σ , median \bar{E}_L , and the fraction of sets with negative \bar{E}_L as a function of s_I . Each gray dot is obtained from one trial of 200 sets. There are 20 trials, and the thick line connects the median values.

range of the Pöschl–Teller potential. For concreteness, we set $\gamma = 1$, $\mu = 1$ in this work.

We use a transformer-based neural network for the trial wave function (Psiformer), consisting of L transformer layers, each with n_H attention heads and embedding dimension h_H [12]. We make two important modifications relative to the original Psiformer: (1) the activation function in the MLP is GeLU rather than tanh, and (2) the SoftMax in the attention mechanism is replaced with StableMax [18]. These modifications improve the stability of the optimization. The output of the final transformer layer is linearly projected to n_D sets of N orbitals, which are then used to construct n_D Slater determinants for antisymmetrizing the fermions. The final wave function is obtained by summing these Slater determinants and multiplying by the Jastrow factor for the harmonic trap, $\mathcal{J}(\mathbf{r}) = \exp(-\alpha^2 \sum_i^N r_i^2)$, where α is a variational parameter. Mathematical details of the neural-network wave function are provided in the End Matter (EM).

Particle configurations \mathbf{r} are drawn from $|\Psi_\theta(\mathbf{r})|^2$ using the Metropolis–Hastings algorithm [5] (EM). The NN wave function is optimized using AdamW with weight decay [19], a robust optimizer that is widely used for

training neural networks. An optimization step alternates between computing the gradient of the loss function with respect to the parameters over batches of size n_{batch} and updating the parameters until all samples are used. A new set of samples is then drawn for the next step. Optimization is stopped when the standard deviation of the local energy, σ_L , falls below 0.01. During optimization, the parameters are saved whenever σ_L reaches a new minimum. If numerical overflow occurs at any step, the parameters are reverted to the most recently saved values. The optimization also stops if σ_L fails to reach a new minimum for 1000 consecutive steps, or if numerical overflow persists for more than 20 reverts.

The weights of the NN wave functions are initialized with random values drawn from a truncated normal distribution with mean 0 and standard deviation s_I , discarding values outside $\pm 2 s_I$ [20]. Biases are initialized to 0. The Jastrow factor parameter α is initialized to 0.7.

We use the simple case of $N_\uparrow = 1$ and $N_d = 1$ as a benchmark for investigating the VMC algorithm. The eigenstates can be obtained by separation of variables into center-of-mass and relative coordinates (EM).

Results.– We can illustrate the PE property of trial

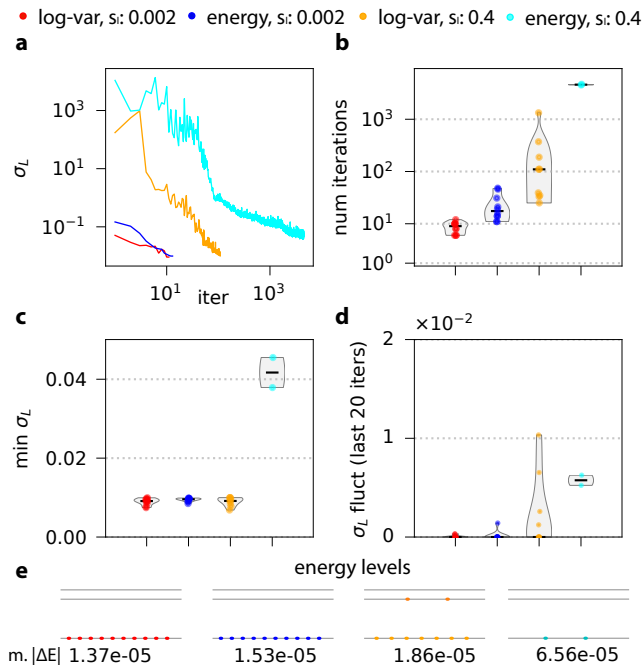


FIG. 2. **Comparison of log-variance minimization and mean-energy minimization for $N_\uparrow = 1, N_\downarrow = 1$.** $(L, n_H, h_H) = (2, 2, 2)$. The neural-network wave functions are randomly initialized with $s_I = 0.002$ (red, blue) or $s_I = 0.4$ (orange, cyan). **a**. Examples of σ_L as a function of iteration number for log-variance minimization (red, orange) and mean-energy minimization (blue, cyan). **b**. Number of iterations required to reach the stopping criterion. Runs for which σ_L does not decrease below 0.1 are excluded. **c**. Minimum σ_L achieved in the runs. **d**. Mean values of σ_L over the last 20 iterations before stopping. **e**. Energy levels obtained in the runs. The numbers indicate the median values of $|\Delta E|$ relative to those obtained by exact diagonalization. The black lines in the violin plots in **b-d** show the medians.

wave functions by constructing simple examples; details are provided in the EM. Importantly, the PE property emerges in neural-network wave functions within certain parameter regimes. We demonstrate this for a network with $(L, n_H, h_H) = (2, 2, 2)$. Initializing neural-network wave functions with small s_I tends to produce smooth wave functions, whereas large s_I tends to produce more jagged wave functions that can exhibit the PE property (Fig.1). We illustrate this for s_I ranging from 0.002 to 0.4. For each s_I , we generate 200 sets of 200,000 Monte Carlo samples from the neural-network wave function, yielding distributions of σ_L and \bar{E}_L . Figure 1a shows these distributions, together with the spatial probability distributions of the up- and down-spin particles. The spatial distributions exhibit broad blobs, suggesting that the neural-network wave function is smooth. Most values of σ_L are smaller than 1, and the values of \bar{E}_L are tightly clustered around 1.96.

In contrast, for $s_I=0.4$ (Fig. 1b), the spatial distributions exhibit finer structures. The values of σ_L are



FIG. 3. **Obtaining the energy spectrum for $N_\uparrow = 1, N_\downarrow = 1$.** $(L, n_H, h_H) = (3, 5, 5)$, and $S_I = 0.2$. Different runs converge to different energy levels. Excluding energies obtained in previous runs leads to new energy levels.

broadly distributed with a heavy tail, and \bar{E} can be negative for some sets of samples. These are hallmarks of the PE property. We quantify the spread of the σ_L distribution by $s_\sigma = (\max \sigma_L - \min \sigma_L) / \text{median } \sigma_L$. For this case, we obtain $s_\sigma = 41.1$. The median value of σ_L is 5.21×10^2 , indicating that the NN wave function is far from an eigenstate.

Increasing s_I progressively produces NN wave functions that more strongly display PE property, as shown in Fig. 1c. We systematically varied s_I from 0.002 to 0.4. For each value of s_I , we generated 200 sets and repeated this procedure 20 times. We then plotted the median of σ_L , the spread s_σ , the median of \bar{E}_L , and the fraction of sets with negative \bar{E} . All of these measures increase with s_I .

The PE property of NN wave functions can introduce large sample-to-sample fluctuations in σ_L^2 and \bar{E}_L . This poses a challenge for energy minimization, especially because some samples can have energies lower than the ground-state energy, causing the learning process to drive the NN wave functions further away from the ground state. In contrast, minimizing the log-variance drives the NN wave functions toward eigenstates regardless of these fluctuations [21, 22].

We illustrate these points using the case $N_\uparrow = 1$ and $N_\downarrow = 1$, with $(L, n_H, h_H) = (2, 2, 2)$ (Fig.2). We compare minimizing the log-variance and the energy. Initialization with $s_I = 0.002$ produces smooth NN wave functions (Fig.1a). Both log-variance and energy minimization lead to convergence, with σ_L reaching 0.01. We compared a set of learning rates and found that 10^{-4} and 5×10^{-5} work well for minimizing the log-variance and the energy, respectively (EM, Fig.S1). Ten runs with these learning rates are shown in Fig.2. Overall, log-variance minimization reached convergence faster than energy minimization. All runs converged to the ground state.

The situation is markedly different with $s_I = 0.4$ initialization, which is expected to produce NN wave functions with the PE property (Fig. 1b). For log-variance minimization, 9/10 runs converged to σ_L below 0.01, although the numbers of iterations were much larger than in the previous case. One run failed to converge to σ_L below 0.1 within 5000 iterations and is excluded. Two of the runs converged to the excited state. In contrast, energy minimization struggled to converge. Only 2/10 runs converged to σ_L below 0.1 within 5000 iterations,

and none reached below 0.01. These results show that log-variance minimization is much more robust than energy minimization in overcoming the PE property of NN wave functions.

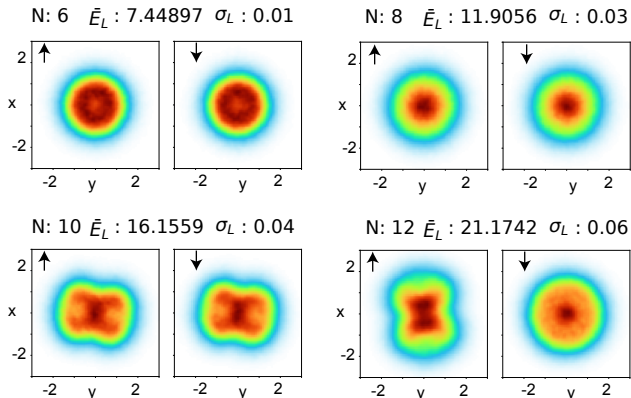


FIG. 4. **Increasing system size.** Here, $N = N_\uparrow + N_\downarrow$ with $N_\uparrow = N_\downarrow$. Particle density, \bar{E}_L , and σ_L are shown for $N = 6, 8, 10, 12$. The network structure was $(L, n_H, h_H) = (5, 5, 5)$ for $N = 6$ and $(L, n_H, h_H) = (5, 5, 10)$ for the other system sizes.

We can exploit the robustness of log-variance minimization to obtain the energy spectrum by initializing the NN wave function with a large s_I . This is demonstrated for the case $N_\uparrow = 1$ and $N_\downarrow = 1$. The network architecture was $(L, n_H, h_H) = (3, 5, 5)$ (Fig. 3). The NN wave function was initialized with $s_I = 0.2$, and the learning rate was initially set to 10^{-4} , then reduced to 5×10^{-5} once σ_L reached 0.05. Across 10 training runs, the learning converged to five distinct energy levels (Fig. 3, left). Interestingly, the ground state was not reached.

The search for the energy spectrum can be accelerated by excluding energy levels that have already been obtained. We propose the following modified loss:

$$\log(\sigma_L^2 + \gamma) - \frac{\beta}{\sigma_{excl}^2} \sum_k \text{softplus}(\sigma_{excl}^2 - \sigma_{Lk}^2) \log(\sigma_{Lk}^2 + \gamma).$$

Here, $\text{softplus}(x) = \log(1 + e^x)$ is a smoothed version of the ReLU function: it approaches 0 for negative x and approaches x for positive x . σ_{Lk} is the variance of $E_L - E_k$, where E_k is an energy level that has already been obtained and is therefore to be excluded. The parameter σ_{excl}^2 controls the extent of this exclusion. Because of the softplus factor, the exclusion term is effective only when $\sigma_{Lk}^2 < \sigma_{excl}^2$, that is, when the sampled E_L values are close to E_k .

The idea is that if the NN wave function approaches the eigenstate at E_k , the loss becomes large, so the learning dynamics is driven away from this state. The parameter β must be large enough to overwhelm the $\log(\sigma_L^2 + \gamma)$ term. We find that $\beta = 5$ and $\sigma_{excl}^2 = 0.5$ work well.

With this modified loss function, all 10 runs converged to the ground state when all five energy levels from the first 10 runs were excluded (Fig. 3, right).

Log-variance minimization works well as the system size increases. Examples with total particle numbers $N = 6, 8, 10, 12$, with $N_\uparrow = N_\downarrow$, are shown in Fig. 4. As the number of particles increases, the network size must also increase, and more iterations are required to achieve good convergence. The network sizes were $(L, n_H, h_H) = (5, 5, 5)$ for the $N = 6$ case and $(L, n_H, h_H) = (5, 5, 10)$ for the others. In general, convergence to $\sigma_L \approx 0.5$ was relatively fast, whereas convergence to values below 0.1 required substantially more iterations. The minimum σ_L also tends to increase with increasing N .

Discussion.—The PE property of neural-network wave functions can be reduced by initializing the network weights with a small standard deviation s_I . Another approach is to precondition the neural-network wave function using mean-field reference states such as Hartree–Fock, as is often done in VMC simulations of atoms and molecules [10, 23]. It is worthwhile to try different values of s_I for initialization, as good initializations often promote faster convergence in training deep neural networks [24]. For obtaining ground states, combining log-variance minimization with energy minimization remains a viable possibility.

The robustness of log-variance minimization against the PE property allows convergence to different excited states from run to run when the neural-network wave functions are initialized with large s_I . Using the exclusion method that we propose, different energy levels can be obtained in different runs. This approach to obtaining the energy spectrum is much simpler than existing methods for computing excited states, such as penalizing wave-function overlaps [25] or expanding the system size [13].

Minimizing the log-variance preserves the gradient information as the variance becomes small and is therefore more effective than minimizing the variance itself. The minimization can be performed using simple first-order optimization techniques such as AdamW [19], which is among the most commonly used methods for training AI models, including the large language model GPT-3 [26]. Compared to second-order optimization methods such as KFAC, which are widely used for training neural-network wave functions [11], first-order methods are easier to implement and less memory intensive, thereby facilitating scaling to larger system sizes.

In conclusion, we have shown that log-variance minimization with VMC can control the expressiveness of neural-network wave functions and facilitate the computation of energy spectra in many-body quantum systems.

Acknowledgments.—This research was supported by the Faculty Upskilling Fellowship in AI and Quantum Sciences, awarded by the Penn State Institute for Computational and Data Sciences. I thank Jainendra Jain, Mytraya Gattu, and Chaoxing Liu for useful discussions.

-
- [1] B. M. Austin, D. Y. Zubarev, and W. A. Lester Jr, Quantum monte carlo and related approaches, *Chemical reviews* **112**, 263 (2012).
- [2] W. M. Foulkes, L. Mitás, R. Needs, and G. Rajagopal, Quantum monte carlo simulations of solids, *Reviews of Modern Physics* **73**, 33 (2001).
- [3] R. Needs, M. Towler, N. Drummond, P. López Ríos, and J. Trail, Variational and diffusion quantum monte carlo calculations with the casino code, *The Journal of chemical physics* **152** (2020).
- [4] S. Giorgini, L. P. Pitaevskii, and S. Stringari, Theory of ultracold atomic fermi gases, *Reviews of Modern Physics* **80**, 1215 (2008).
- [5] S. Chib and E. Greenberg, Understanding the metropolis-hastings algorithm, *The american statistician* **49**, 327 (1995).
- [6] D. Ceperley, G. V. Chester, and M. H. Kalos, Monte carlo simulation of a many-fermion study, *Physical Review B* **16**, 3081 (1977).
- [7] C. Umrigar, K. Wilson, and J. Wilkins, Optimized trial wave functions for quantum monte carlo calculations, *Physical Review Letters* **60**, 1719 (1988).
- [8] P. R. Kent, R. Needs, and G. Rajagopal, Monte carlo energy and variance-minimization techniques for optimizing many-body wave functions, *Physical Review B* **59**, 12344 (1999).
- [9] C. Umrigar and C. Filippi, Energy and variance optimization of many-body wave functions, *Physical review letters* **94**, 150201 (2005).
- [10] J. Hermann, Z. Schätzle, and F. Noé, Deep-neural-network solution of the electronic schrödinger equation, *Nature Chemistry* **12**, 891 (2020).
- [11] D. Pfau, J. S. Spencer, A. G. Matthews, and W. M. C. Foulkes, Ab initio solution of the many-electron schrödinger equation with deep neural networks, *Physical review research* **2**, 033429 (2020).
- [12] I. von Glehn, J. S. Spencer, and D. Pfau, A self-attention ansatz for ab-initio quantum chemistry, *arXiv preprint arXiv:2211.13672* (2022).
- [13] D. Pfau, S. Axelrod, H. Sutterud, I. von Glehn, and J. S. Spencer, Accurate computation of quantum excited states with neural networks, *Science* **385**, eadn0137 (2024).
- [14] Y. Teng, D. D. Dai, and L. Fu, Solving and visualizing fractional quantum hall wavefunctions with neural network, *arXiv preprint arXiv:2412.00618* (2024).
- [15] Y. Qian, T. Zhao, J. Zhang, T. Xiang, X. Li, and J. Chen, Describing landau level mixing in fractional quantum hall states with deep learning, *Physical Review Letters* **134**, 176503 (2025).
- [16] A. J. Morris, P. López Ríos, and R. Needs, Ultracold atoms at unitarity within quantum monte carlo methods, *Physical Review A—Atomic, Molecular, and Optical Physics* **81**, 033619 (2010).
- [17] M. Holten, L. Bayha, K. Subramanian, C. Heintze, P. M. Preiss, and S. Jochim, Observation of pauli crystals, *Physical Review Letters* **126**, 020401 (2021).
- [18] L. Prieto, M. Barsbey, P. A. Mediano, and T. Birdal, Grokking at the edge of numerical stability, *arXiv preprint arXiv:2501.04697* (2025).
- [19] I. Loshchilov and F. Hutter, Decoupled weight decay regularization, *arXiv preprint arXiv:1711.05101* (2017).
- [20] A. Radford, K. Narasimhan, T. Salimans, I. Sutskever, *et al.*, Improving language understanding by generative pre-training, (2018).
- [21] P. R. C. Kent, *Techniques and applications of quantum Monte Carlo*, Ph.D. thesis, University of Cambridge (1999).
- [22] C. Umrigar, J. Toulouse, C. Filippi, S. Sorella, and R. G. Hennig, Alleviation of the fermion-sign problem by optimization of many-body wave functions, *Physical review letters* **98**, 110201 (2007).
- [23] M. Scherbela, L. Gerard, and P. Grohs, Towards a transferable fermionic neural wavefunction for molecules, *Nature Communications* **15**, 120 (2024).
- [24] S. Fort and A. Scherlis, The goldilocks zone: Towards better understanding of neural network loss landscapes, in *Proceedings of the aaai conference on artificial intelligence*, Vol. 33 (2019) pp. 3574–3581.
- [25] M. T. Entwistle, Z. Schätzle, P. A. Erdman, J. Hermann, and F. Noé, Electronic excited states in deep variational monte carlo, *Nature Communications* **14**, 274 (2023).
- [26] T. Brown, B. Mann, N. Ryder, M. Subbiah, J. D. Kaplan, P. Dhariwal, A. Neelakantan, P. Shyam, G. Sastry, A. Askell, *et al.*, Language models are few-shot learners, *Advances in neural information processing systems* **33**, 1877 (2020).

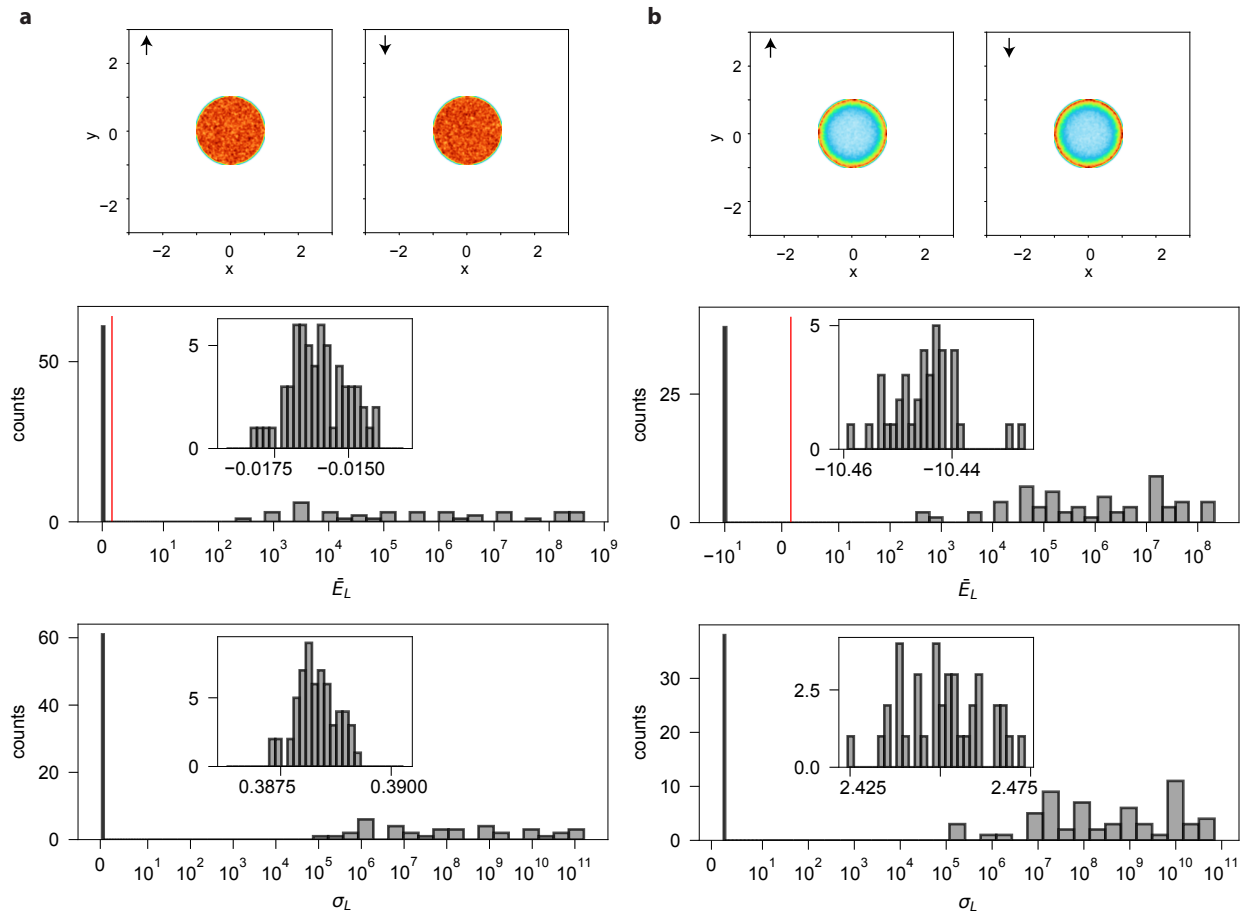


FIG. S1. Particle densities and distributions of \bar{E}_L and σ_L for 100 sample sets with $N_\uparrow = 1$ and $N_\downarrow = 1$, obtained from two trial wave functions defined by **a** Eq. 1 and **b** Eq. 2. The insets show enlarged views of the low- \bar{E}_L and low- σ_L regions. The red line denotes the ground-state energy.

END MATTER

Neural network wave function.—We use a transformer-based neural network for the trial wave function (Psi-former) [12]. Mathematically, the network can be regarded as a series of transformations of the position vector \mathbf{r}_i for each particle, parameterized by the network weights and biases (denoted by \mathbf{W} 's and \mathbf{b} 's in the following passages).

The network consists of N processing streams, one for each particle. In each stream, the particle position \mathbf{r}_i is linearly projected into a vector \mathbf{R} in an M -dimensional embedding space, which is subsequently transformed by the transformer layers. The stream is influenced by the other particles through the attention mechanism.

Each transformation layer consists of the following sequence: (1) layer normalization, $\mathbf{R}_1 = \text{LayerNorm}(\mathbf{R})$, such that the elements of \mathbf{R}_1 have mean 0 and variance 1; (2) addition of an attention vector \mathbf{A} , computed from information from other particles, yielding $\mathbf{R}_2 = \mathbf{R}_1 + \mathbf{A}$; (3) layer normalization, $\mathbf{R}_3 = \text{LayerNorm}(\mathbf{R}_2)$; (4) a

multilayer perceptron (MLP) with two hidden layers of size $4M$, $\mathbf{R}_4 = \text{MLP}(\mathbf{R}_3)$; (5) a residual connection producing the layer output, $\mathbf{R}' = \mathbf{R}_2 + \mathbf{R}_4$. The attention vector \mathbf{A} is computed using n_H attention heads, where the embedding dimension of each head is h_H . We enforce $M = n_H h_H$. The computation follows the standard attention mechanism, which incorporates information from the other particles into the current stream.

Monte Carlo sampling.—We used 2048 walkers, each generating 100 samples, resulting in 204800 samples overall. Each walker begins from a random configuration and generates a sequence of accepted configurations. To reduce dependence on the initial conditions, the first 1000 configurations are discarded, and to mitigate correlations, every 10th configuration thereafter is recorded as a sample. The acceptance ratio was maintained between 0.2 and 0.8.

Simple examples of wave functions with PE property.—Consider the following trial wave function for $N_\uparrow = 1$ and

$N_{\downarrow} = 1$:

$$\Psi_{\theta} = \mathcal{N} \tanh\left(\frac{1-\rho_1}{d}\right) \tanh\left(\frac{1-\rho_2}{d}\right), \quad (1)$$

where ρ_1 and ρ_2 denote the radial positions of the particles, \mathcal{N} is the normalization factor, and d is a parameter. The function defines two plateau regions: for $(\rho_1 < 1, \rho_2 < 1)$ we have $\Psi_{\theta} \approx 1$, while for $(\rho_1 > 1, \rho_2 > 1)$ we have $\Psi_{\theta} \approx 0$. Small d creates a sharp crease between the plateau regions.

As a concrete example, we set $d = 10^{-7}$, drew 100 sets of 200,000 samples from this trial wave function, and computed \bar{E}_L and σ_L for each set. The distributions of \bar{E}_L and σ_L are highly skewed (Fig. S1a). A fraction of 0.61 of the sets have \bar{E}_L smaller than the ground-state energy and exhibit small σ_L (inserts). Over all sets, the median value of \bar{E}_L is -0.015 , and the median of σ_L is 0.39. Increasing d (reducing the edge sharpness) decreases the fraction of sets with \bar{E}_L below the ground-state energy, whereas decreasing d (sharpening the edge) increases this fraction.

It is possible to construct trial wave functions that yield negative kinetic energy in the plateau regions. If the curvature of Ψ_{θ} has the same sign as Ψ_{θ} itself, then the ratio $\nabla^2\Psi_{\theta}/\Psi_{\theta}$ becomes positive, which renders the kinetic-energy contribution negative. In this case, a substantial fraction of sample sets can exhibit negative \bar{E}_L . One example is

$$\Psi_{\theta} = \mathcal{N} \tanh\left(\frac{1-\rho_1}{d}\right) \tanh\left(\frac{1-\rho_2}{d}\right) (\rho_1^4 + \rho_2^4), \quad (2)$$

which is obtained from Eq. 1 by including an additional factor that introduces positive curvature in the plateau region.

We again set $d = 10^{-7}$ and drew 100 sets of 200,000 samples. A fraction of 0.38 of the sets have \bar{E}_L smaller than -10 , which is far below the minimum energy allowed by the attractive potential (Fig. S1b). Increasing the power of the polynomial factor in Eq. 2 makes \bar{E}_L more negative, while simultaneously decreasing the fraction of sample sets with negative \bar{E}_L . For example, using the factor $(\rho_1^{20} + \rho_2^{20})$, a fraction of 0.04 of the sets have negative \bar{E}_L , with values around -211 .

Energy levels for $N_{\uparrow} = 1$, $N_{\downarrow} = 1$.—We make the coordinate transformation $\mathbf{r}_1 = \mathbf{R} + \rho/2$, $\mathbf{r}_2 = \mathbf{R} - \rho/2$, where \mathbf{R} is the center-of-mass coordinates, and ρ is the vector from particle 1 to particle 2. Wave function can be separated $\Psi(\mathbf{r}_1, \mathbf{r}_2) = \phi(\mathbf{R})\psi(\rho)$. The equation for \mathbf{R} is that of mass 2 particle in the 2D harmonic trap, and the

eigenvalues are $E_R = n + 1$, $n = 0, 1, \dots$. Expressing in polar coordinates $\boldsymbol{\rho} = (\rho, \theta)$ and $\psi(\boldsymbol{\rho}) = \eta(\rho)e^{im\theta}$, where m is the angular momentum quantum number, we find

$$\left[-\frac{d^2}{d\rho^2} - \frac{1}{\rho} \frac{d}{d\rho} + \frac{m^2}{\rho^2} + \frac{1}{4}\rho^2 - \frac{1}{\cosh^2(\rho)}\right] \eta(\rho) = E_{\rho}\eta(\rho). \quad (3)$$

The boundary condition is $\eta'(0) = 0$, $\eta(\infty) = 0$.

The equation is solved numerically by discretizing the domain $(0, \rho_{\max} = 10.0)$ into $N = 2000$ equally spaced points. The differential operators are approximated using the second-order central-difference scheme, and the resulting discretized equations are formulated as a matrix eigenvalue problem. We systematically varied m from 0 to 10, and for each value of m we computed the lowest 10 eigenvalues corresponding to the quantum number l . The lowest energy levels are summarized in Table I. To assess numerical accuracy, the calculation was repeated with halved grid resolution ($N = 1000$), and the absolute differences between the two sets of results were taken as estimates of the numerical error.

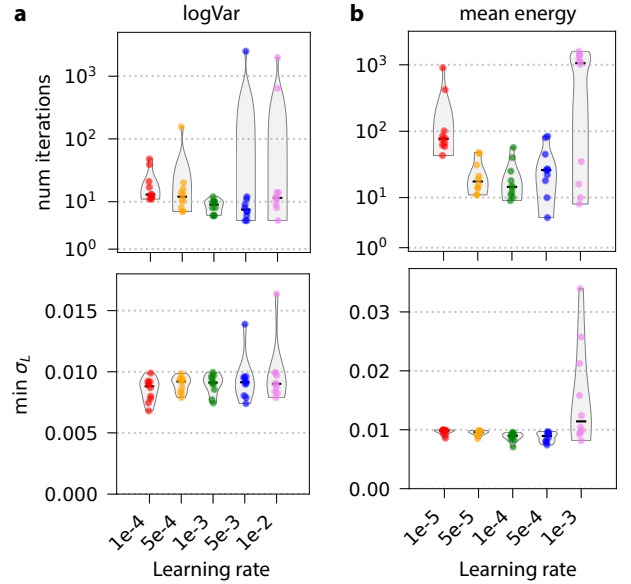


FIG. S2. **Learning dynamics vs. the learning rate for $N_{\uparrow} = 1$, $N_{\downarrow} = 1$, and $S_I = 0.002$.** (L, n_H, h_H) = (2, 2, 2). There are 10 runs for each learning rate. The number of iterations required to reach the stopping criterion and the minimum σ_L attained are shown as violin plots for (a) minimizing the log-variance and (b) minimizing the mean energy. The black lines in the violin plots show the medians.

| (n, m, l) | E | error | (n, m, l) | E | error | (n, m, l) | E | error |
|-----------|----------|----------------------|-----------|----------|----------------------|-----------|----------|----------------------|
| (0, 0, 0) | 1.592687 | 1.1×10^{-5} | (1, 0, 0) | 2.592687 | 1.1×10^{-5} | (0, 1, 0) | 2.830440 | 5.5×10^{-6} |
| (2, 0, 0) | 3.592687 | 1.1×10^{-5} | (0, 0, 1) | 3.800086 | 9.4×10^{-6} | (1, 1, 0) | 3.830440 | 5.5×10^{-6} |
| (0, 2, 0) | 3.923556 | 4.8×10^{-6} | (3, 0, 0) | 4.592687 | 1.1×10^{-5} | (1, 0, 1) | 4.800086 | 9.4×10^{-6} |

TABLE I. Lowest energy levels for $N_{\uparrow} = 1$, $N_{\downarrow} = 1$. n, m, l are quantum numbers.